

Domain wall resistance in CoFeB-based heterostructures with interface Dzyaloshinskii-Moriya interaction

Yuto Ishikuro¹, Masashi Kawaguchi¹, Yong-Chang Lau^{1,2}, Yoshinobu Nakatani³ and Masamitsu Hayashi^{1,2*}

¹*Department of Physics, The University of Tokyo, Bunkyo, Tokyo 113-0033, Japan*

²*National Institute for Materials Science, Tsukuba 305-0047, Japan*

³*University of Electro-Communications, Chofu, Tokyo 182-8585, Japan*

We have studied the domain wall resistance in W/Ta/CoFeB/MgO heterostructures. The Ta layer thickness is varied to control the type of domain walls via changes in the interfacial Dzyaloshinskii Moriya interaction. We find a nearly constant domain wall resistance against the Ta layer thickness. Adding contributions from the anisotropic magnetoresistance, spin Hall magnetoresistance and anomalous Hall effect describe well the domain wall resistance of the thick Ta layer films. However, a discrepancy remains for the thin Ta layer films wherein chiral Néel-like domain walls are found. These results show the difficulty of studying the domain wall type from resistance measurements.

*Email: hayashi@phys.s.u-tokyo.ac.jp

The Dzyaloshinskii–Moriya interaction (DMI)^{1,2} at the interface between a heavy metal (HM) and a ferromagnetic metal (FM) layers³ enables stabilization of homochiral Néel domain walls (DWs)⁴. Néel DWs can be driven by current with high velocity via the spin Hall effect of the HM layer⁵⁻⁸. Significant effort has been made to develop means to determine the character of the DWs, whether they form a Néel or Bloch walls, and the strength of the DMI⁹⁻¹⁴. It has been demonstrated previously that the anisotropic magnetoresistance (AMR) of the FM layer can be used to identify the structure and type of DWs^{15,16}. Direct determination of the DW type using resistance measurements allows simple evaluation of the DMI, including its spatial distribution. Local changes in the DMI at the HM/FM interface has been reported to be non-negligible^{17,18}.

Here we study DW resistance in Sub/W/Ta/CoFeB/MgO heterostructures. A thin Ta layer is inserted between the W and CoFeB layers to vary the strength of the DMI. We compare the DW resistance with calculations that includes contributions from the AMR, the spin Hall magnetoresistance (SMR)¹⁹⁻²² and the anomalous Hall effect (AHE). We find that such estimation agrees well with the DW resistance for the thick Ta layer films; however, a discrepancy remains for the thinner Ta layer films. Other contribution to the DW resistance, including the recently discovered chiral DW resistance²³, may account for the discrepancy. Despite the large SMR, these results show the difficulty of evaluating the type of DW using simple resistance measurements.

Films are grown on Si substrates using magnetron sputtering. Figure 1(a) shows schematic illustration of the film stack used here, i.e. Sub./3 W/*d* Ta/1 CoFeB/2 MgO/1 Ta (units in nanometer). The thickness of the Ta insertion layer *d* is varied to control the size of the DMI. All films are annealed at 300 degree C for 1 hour. Optical lithography and Ar ion milling are used to form wires and Hall bars. The width and length of the wires are typically $\sim 5\ \mu\text{m}$ and $\sim 30\ \mu\text{m}$, respectively. The width (*w*) and the distance (*L*) between the longitudinal voltage probes of the Hall bars are $\sim 10\ \mu\text{m}$ and $\sim 25\ \mu\text{m}$, respectively. Figure 1(b) shows a Kerr

microscopy images of typical wire and Hall bar with the definition of the coordinate axis. Voltage pulses are applied to the wire to nucleate DWs. The current associated with the pulse flows along the x direction. External magnetic fields are applied along the x , y , and z directions, which we refer to as H_x , H_y , and H_z , respectively.

Figures 1(c) and 1(d) show the Ta layer thickness dependence of the saturation magnetization per unit volume M_s and the magnetic anisotropy energy density K_{eff} , respectively. M_s and K_{eff} are evaluated with vibrating sample magnetometry (VSM) using unpatterned films. Both M_s and K_{eff} decrease as d is increased. We infer that intermixing of Ta and CoFeB at the interface causes such variation²⁴.

The transport properties of the films are summarized in Figs. 1(e) and 1(f). Figure 1(e) shows the Ta layer thickness dependence of the anomalous Hall angle $\varphi_{\text{AHE}}^{\text{eff}}$ measured using the Hall bars. The anomalous Hall resistance ΔR_{xy} , obtained from the difference of the Hall resistance R_{xy} when the magnetization of the CoFeB layer points along $+z$ and $-z$, is divided by the longitudinal resistance R_{xx} and multiplied by a geometrical factor (L/w) to estimate $\varphi_{\text{AHE}}^{\text{eff}}$, i.e. $\tan(\varphi_{\text{AHE}}^{\text{eff}}) = \frac{1}{2} \frac{\Delta R_{xy}}{R_{xx}} \frac{L}{w}$. $\varphi_{\text{AHE}}^{\text{eff}}$ decreases with increasing d due to current shunting into the Ta layer. The Ta layer thickness dependence of the AMR and the SMR are shown in Fig. 1(f). The longitudinal resistance of the Hall bars measured against magnetic field directed along the x , y , and z axes are defined as R_{xx}^x , R_{xx}^y , and R_{xx}^z , respectively. Setting $\Delta R_{xx}^x = R_{xx}^x - R_{xx}^z$ and $\Delta R_{xx}^y = R_{xx}^y - R_{xx}^z$, the magnetoresistance ratios $r_{\text{AMR}} = \Delta R_{xx}^x / R_{xx}^z$ due to AMR and $r_{\text{SMR}} = \Delta R_{xx}^y / R_{xx}^z$ caused by SMR are plotted as a function of d in Fig. 1(f). The AMR of the heterostructures is negligible compared to the SMR²². SMR decreases with increasing Ta layer thickness mostly due to current shunting effect (into Ta).

The DMI is measured using the in-plane field dependence of the current induced anomalous Hall loop shift¹⁴ and the DW velocity^{6,7,25}. For the former, R_{xy} vs. H_z is measured under application of a DC bias current I_{DC} . Figure 2(a) shows representative R_{xy} - H_z loops for a device with $d \sim 0.1$ nm ($H_x = -1100$ Oe and $I_{DC} = \pm 6$ mA). When a positive (negative) current is applied, the center of the hysteresis shifts to positive (negative) H_z . The shift of the loop center is defined as H_{eff}^z . The inset to Fig. 2(b) shows H_{eff}^z as a function of I_{DC} for the same device and H_x . H_{eff}^z scales linearly with I_{DC} . We fit the H_{eff}^z vs. I_{DC} with a linear function: the slope of the fitted function is plotted against H_x in Fig. 2(b). Note that here we have converted the bias current I_{DC} to the current density that flows through the HM layer (J_e). The H_x at which H_{eff}^z/J_e saturates corresponds to the DM exchange field H_{DM} ¹⁴. We find $H_{DM} \sim 200$ Oe for devices with $d \sim 0.1$ nm.

The in-plane field dependence of the current induced DW velocity is also measured to estimate H_{DM} . The distance a DW moved when voltage pulses are applied is measured using a Kerr microscopy. The DW velocity is estimated by dividing the distance the DW traveled by the pulse length. Fig. 2(c) shows the velocity for up-down (black squares) and down-up (red circles) DWs plotted as a function of H_x . From these plots, H_{DM} is estimated from the H_x at which the velocity becomes zero. Linear lines are fitted to the data to estimate H_{DM} .

The DM exchange constant D is calculated from H_{DM} using the following relation $D = \mu_0 M_s H_{DM} \Delta$. $\Delta = \sqrt{\frac{A}{K_{eff}}}$, where A is the exchange stiffness and here we used $A = 31$ pJ/m from previous reports²⁶. M_s and K_{eff} are obtained from interpolating the data shown in Figs. 1(c) and 1(d). The black squares (green circles) in Fig. 2(d) show D estimated using the anomalous Hall shift (DW velocity). D decreases from ~ 0.2 mJ/m² to ~ 0 mJ/m² with increasing Ta layer thickness.

The DW resistance is obtained by nucleating multiple DWs into the wire and measuring the wire's resistance. DWs are nucleated with a single voltage pulse (~ 28 V, 100 ns) applied to the wire without any magnetic field. After nucleation, H_z is applied to change the number of DWs in the wire. H_z is then reduced to zero and the resistance and the magnetic state of the wire are studied using transport and Kerr measurements, respectively. $|H_z|$ is subsequently increased to further change the number of DWs. This process is repeated with increasing H_z to annihilate all DWs in the wire.

Figure 3(a) shows representative Kerr images of the wire when H_z is varied. The associated change of the wire resistance is shown in Fig. 3(b). We record the change in the wire resistance (δR) when the number of DWs in the wire changes due to the application of H_z (note that the resistance is measured at zero field). The DW resistance (ΔR) is obtained by dividing δR with the number of DWs annihilated at the corresponding field. We find little dependence of ΔR on H_z . Such measurement is repeated for more than 100 times to gain statistics of the DW resistance. Normalized histograms of ΔR for films with $d \sim 0.1, 0.5$ and 0.8 nm are shown in Fig. 4(a). The histograms are fitted with a Gaussian function to find the mean value, which is plotted in Fig. 4(b) (black squares) as a function of d . ΔR is positive for all devices regardless of the Ta layer thickness. The value of DW resistance is ~ 20 m Ω .

To account for the DW resistance observed, we first examine contributions from the SMR and AMR. The magnetization rotates within the zx (zy) plane across a Néel (Bloch) DW leading to a non-zero $x(y)$ projection of the magnetization at the DW where the AMR (SMR) contribution is relevant. As shown in Fig. 1(f), the magnitude of AMR is orders of magnitude smaller than SMR and thus we may neglect its influence on ΔR . The two solid lines in Fig. 4(b) show the range of DW resistance when contributions of SMR are taken into account. The upper blue (lower red) line indicates the level of ΔR provided the DWs are Néel (Bloch) type. As evident,

contribution from SMR on ΔR is smaller than what has been observed experimentally (Fig. 4(b), black squares) despite the relatively large SMR found in this system. Moreover the DW resistance due to SMR is negative: i.e. the uniformly magnetized state has a larger resistance compared to the state containing DWs. Thus clearly ΔR found in the experiments have a different origin.

Next, the DW resistance that occurs due to the anomalous Hall effect (AHE)²⁷⁻²⁹ is considered. Electrons are deflected from the current flow direction when the AHE is present in perpendicularly magnetized systems. Similar deflections occur when perpendicular magnetic field is applied to conductors via the Hall effect. Across a domain wall, electrons will experience deflection in opposite directions, resulting in an abrupt change of their trajectory. Such an abrupt trajectory change results in additional resistance at the DW: the effect is proportional to the square of the anomalous Hall angle of the FM layer. We use finite element simulation to estimate the AHE induced DW resistance. The electric potential distribution in the wire is calculated with and without a DW. (The length and width of the wire is varied to exclude geometrical effects on the DW resistance.) The change in the wire resistance due to the presence of a DW is obtained as the AHE induced DW resistance. Measured values of the d -dependent anomalous Hall angle (φ_{AHE}) of the CoFeB layer are used in the simulations. φ_{AHE} is obtained from $\varphi_{\text{AHE}}^{\text{eff}}$ by excluding current shunting into other conducting layers: the resistivity of the three conducting layers (W, Ta, CoFeB) used in the calculations are ~ 120 , ~ 200 and $\sim 160 \mu\Omega \text{ cm}$ for W, Ta and CoFeB, respectively²⁵. The calculated DW resistance due to AHE is plotted by the green circles in Fig. 4(b). ΔR due to AHE is positive and its magnitude is close to that of the experimental results. We find a relatively good agreement between the experiments and the combined contributions from the AHE and SMR for the thick Ta layer films where D is small and the DWs are Bloch-type. However, a discrepancy between the two

(experiments vs. AHE and SMR) remains for the thinner Ta layer films: a negative DW resistance of the order $\sim 10 \text{ m}\Omega$ is needed to account for the difference.

One well known DW resistance that may influence the measurements is the so-called intrinsic contribution due to spin accumulation at the DW^{30,31}. The intrinsic DW resistance is expected to increase as the DW width becomes smaller. As K_{eff} increases with decreasing Ta layer thickness, the DW width, which scales with $(K_{\text{eff}})^{-\frac{1}{2}}$, becomes smaller for thinner Ta layer films. As the intrinsic contribution is typically positive^{32,33}, we infer that this effect cannot account for the difference of ΔR between the experiments and the estimation of the thinner Ta layer films.

Recently, it has been reported that a chiral DW resistance appears in system with large spin orbit coupling²³. Provided a Rashba-like Hamiltonian can describe the electronic states of the heterostructure, an additional DW resistance emerges only when the magnetic configuration is a chiral Néel type. A theoretical model predicts that the DW resistance is negative for chiral magnetic structures²³. We therefore infer that the chiral DW resistance may partly account for the difference between the experiments and the estimation for the thin Ta layer films. According to Ref. [23] the chiral DW resistance is expressed as $R_{\text{chi}} \sim (\pi R_{\text{DW}} \Delta D) / (2A)^{23,34}$. We estimate $R_{\text{chi}} \sim 2 \text{ m}\Omega$ for chiral Néel DWs if we take R_{DW} from the thicker Ta films wherein no chiral DW resistance is assumed. As a few approximations are made in the formula above, further investigation is required to clarify contribution from the chiral DW resistance.

In summary, we have studied the DW resistance in W/Ta/CoFeB/MgO heterostructures as a function of Ta insertion layer thickness. The thickness of the Ta layer influences the DW type (Néel-like walls or Bloch walls) via changes in the Dzyaloshinskii Moriya interaction. In contrast, we find the DW resistance shows little variation with the Ta layer thickness. The DW resistance of the thick Ta layer films can be accounted for by taking into consideration the

SMR and AHE of the heterostructures. However, a discrepancy remains for the thin Ta layer films, wherein the DWs are chiral Néel-like DWs. We infer that chiral DW resistance, or other unknown source, contributes to the resistance in such systems. These results show that, despite the large SMR, DW resistance measurements cannot be used to identify the type of DWs.

Acknowledgements

The authors thank Daichi Chiba and Kyung-Jin Lee for discussion on domain wall magnetoresistance. This work was partly supported by JSPS Grant-in-Aids (15H05702, 16H03853), Casio Foundation, and Center of the Spintronics Research Network of Japan. Y.-C.L. is a JSPS international research fellow.

References

- 1 I. E. Dzyaloshinskii, "Thermodynamic Theory of Weak Ferromagnetism in Antiferromagnetic Substances." *Sov. Phys. JETP* **5**, 1259 (1957).
- 2 T. Moriya, "Anisotropic Superexchange Interaction and Weak Ferromagnetism." *Phys. Rev.* **120**, 91 (1960).
- 3 A. Fert, V. Cros, and J. Sampaio, "Skyrmions on the Track." *Nat. Nanotechnol.* **8**, 152 (2013).
- 4 M. Heide, G. Bihlmayer, and S. Blugel, "Dzyaloshinskii-Moriya Interaction Accounting for the Orientation of Magnetic Domains in Ultrathin Films: Fe/W(110)." *Phys. Rev. B* **78** 140403 (2008).
- 5 A. Thiaville, S. Rohart, E. Jue, V. Cros, and A. Fert, "Dynamics of Dzyaloshinskii Domain Walls in Ultrathin Magnetic Films." *Europhys. Lett.* **100** 57002 (2012).
- 6 S. Emori, U. Bauer, S.-M. Ahn, E. Martinez, and G. S. D. Beach, "Current-Driven Dynamics of Chiral Ferromagnetic Domain Walls." *Nat. Mater.* **12**, 611 (2013).
- 7 K.-S. Ryu, L. Thomas, S.-H. Yang, and S. Parkin, "Chiral Spin Torque at Magnetic Domain Walls." *Nat. Nanotechnol.* **8**, 527 (2013).
- 8 S.-H. Yang, K.-S. Ryu, and S. Parkin, "Domain-Wall Velocities of up to 750 M S(-1) Driven by Exchange-Coupling Torque in Synthetic Antiferromagnets." *Nat. Nanotechnol.* **10**, 221 (2015).
- 9 S.-G. Je, D.-H. Kim, S.-C. Yoo, B.-C. Min, K.-J. Lee, and S.-B. Choe, "Asymmetric Magnetic Domain-Wall Motion by the Dzyaloshinskii-Moriya Interaction." *Phys. Rev. B* **88** 214401 (2013).
- 10 S. Emori, E. Martinez, K.-J. Lee, H.-W. Lee, U. Bauer, S.-M. Ahn, P. Agrawal, D. C. Bono, and G. S. D. Beach, "Spin Hall Torque Magnetometry of Dzyaloshinskii Domain Walls." *Phys. Rev. B* **90** 184427 (2014).
- 11 J. P. Tetienne, T. Hingant, L. J. Martinez, S. Rohart, A. Thiaville, L. H. Diez, K. Garcia, J. P. Adam, J. V. Kim, J. F. Roch, I. M. Miron, G. Gaudin, L. Vila, B. Ocker, D. Ravelosona, and V. Jacques, "The Nature of Domain Walls in Ultrathin Ferromagnets Revealed by Scanning Nanomagnetometry." *Nat. Commun.* **6** 6733 (2015).
- 12 K. Di, V. L. Zhang, H. S. Lim, S. C. Ng, M. H. Kuok, J. Yu, J. Yoon, X. Qiu, and H. Yang, "Direct Observation of the Dzyaloshinskii-Moriya Interaction in a Pt/Co/Ni Film." *Phys. Rev. Lett.* **114** 047201 (2015).
- 13 R. Soucaille, M. Belmeguenai, J. Torrejon, J. V. Kim, T. Devolder, Y. Roussigné, S. M. Chérif, A. A. Stashkevich, M. Hayashi, and J. P. Adam, "Probing the Dzyaloshinskii-Moriya Interaction in Cofeb Ultrathin Films Using Domain Wall Creep and Brillouin Light Spectroscopy." *Phys. Rev. B* **94**, 104431 (2016).
- 14 C.-F. Pai, M. Mann, A. J. Tan, and G. S. D. Beach, "Determination of Spin Torque Efficiencies in Heterostructures with Perpendicular Magnetic Anisotropy." *Phys. Rev. B* **93** 144409 (2016).
- 15 M. Hayashi, L. Thomas, C. Rettner, R. Moriya, X. Jiang, and S. S. P. Parkin, "Dependence of Current and Field Driven Depinning of Domain Walls on Their Structure and Chirality in Permalloy Nanowires." *Phys. Rev. Lett.* **97**, 207205 (2006).
- 16 T. Koyama, D. Chiba, K. Ueda, K. Kondou, H. Tanigawa, S. Fukami, T. Suzuki, N. Ohshima, N. Ishiwata, Y. Nakatani, K. Kobayashi, and T. Ono, "Observation of the Intrinsic Pinning of a Magnetic Domain Wall in a Ferromagnetic Nanowire." *Nature Mater.* **10**, 194 (2011).

- 17 S. Woo, K. Litzius, B. Kruger, M.-Y. Im, L. Caretta, K. Richter, M. Mann, A. Krone, R. M. Reeve, M. Weigand, P. Agrawal, I. Lemesch, M.-A. Mawass, P. Fischer, M. Klau, and G. S. D. Beach, "Observation of Room-Temperature Magnetic Skyrmions and Their Current-Driven Dynamics in Ultrathin Metallic Ferromagnets." *Nat Mater* **15**, 501 (2016).
- 18 I. Gross, L. J. Martínez, J. P. Tetienne, T. Hingant, J. F. Roch, K. Garcia, R. Soucaille, J. P. Adam, J. V. Kim, S. Rohart, A. Thiaville, J. Torrejon, M. Hayashi, and V. Jacques, "Direct Measurement of Interfacial Dzyaloshinskii-Moriya Interaction in X|Cofeb|Mgo Heterostructures with a Scanning Nv Magnetometer (X=Ta, Tan, and W)." *Phys. Rev. B* **94**, 064413 (2016).
- 19 H. Nakayama, M. Althammer, Y. T. Chen, K. Uchida, Y. Kajiwara, D. Kikuchi, T. Ohtani, S. Geprags, M. Opel, S. Takahashi, R. Gross, G. E. W. Bauer, S. T. B. Goennenwein, and E. Saitoh, "Spin Hall Magnetoresistance Induced by a Nonequilibrium Proximity Effect." *Phys. Rev. Lett.* **110** 206601 (2013).
- 20 M. Althammer, S. Meyer, H. Nakayama, M. Schreier, S. Altmannshofer, M. Weiler, H. Huebl, S. Gepraegs, M. Opel, R. Gross, D. Meier, C. Klewe, T. Kuschel, J.-M. Schmalhorst, G. Reiss, L. Shen, A. Gupta, Y.-T. Chen, G. E. W. Bauer, E. Saitoh, and S. T. B. Goennenwein, "Quantitative Study of the Spin Hall Magnetoresistance in Ferromagnetic Insulator/Normal Metal Hybrids." *Phys. Rev. B* **87** 224401 (2013).
- 21 Y. T. Chen, S. Takahashi, H. Nakayama, M. Althammer, S. T. B. Goennenwein, E. Saitoh, and G. E. W. Bauer, "Theory of Spin Hall Magnetoresistance." *Phys. Rev. B* **87** 144411 (2013).
- 22 J. Kim, P. Sheng, S. Takahashi, S. Mitani, and M. Hayashi, "Spin Hall Magnetoresistance in Metallic Bilayers." *Phys. Rev. Lett.* **116** 097201 (2016).
- 23 Y. X. Yin, D. S. Han, J. S. Kim, R. Lavrijsen, K. J. Lee, S. W. Lee, K. W. Kim, H. W. Lee, H. J. M. Swagten, and B. Koopmans, "Chiral Magnetoresistance in Pt/Co/Pt Zigzag Wires." *Appl. Phys. Lett.* **110**, 5 122401 (2017).
- 24 J. Sinha, M. Hayashi, A. J. Kellock, S. Fukami, M. Yamanouchi, M. Sato, S. Ikeda, S. Mitani, S. H. Yang, S. S. P. Parkin, and H. Ohno, "Enhanced Interface Perpendicular Magnetic Anisotropy in Ta|Cofeb|Mgo Using Nitrogen Doped Ta Underlayers." *Appl. Phys. Lett.* **102** 242405 (2013).
- 25 J. Torrejon, J. Kim, J. Sinha, S. Mitani, M. Hayashi, M. Yamanouchi, and H. Ohno, "Interface Control of the Magnetic Chirality in Cofeb/Mgo Heterostructures with Heavy-Metal Underlayers." *Nat. Commun.* **5** 4655 (2014).
- 26 M. Yamanouchi, A. Jander, P. Dhagat, S. Ikeda, F. Matsukura, and H. Ohno, "Domain Structure in Cofeb Thin Films with Perpendicular Magnetic Anisotropy." *IEEE Magn. Lett.* **2**, 3000304 (2011).
- 27 L. Berger, "Low-Field Magnetoresistance and Domain Drag in Ferromagnets." *J. Appl. Phys.* **49**, 2156 (1978).
- 28 D. L. Partin, M. Karnezos, Demeneze.Lc, and L. Berger, "Nonuniform Current Distribution in Neighborhood of a Ferromagnetic Domain-Wall in Cobalt at 42k." *J. Appl. Phys.* **45**, 1852 (1974).
- 29 D. Chiba, M. Yamanouchi, F. Matsukura, T. Dietl, and H. Ohno, "Domain-Wall Resistance in Ferromagnetic (Ga,Mn)As." *Phys. Rev. Lett.* **96**, 096602 (2006).
- 30 P. M. Levy and S. F. Zhang, "Resistivity Due to Domain Wall Scattering." *Phys. Rev. Lett.* **79**, 5110 (1997).
- 31 G. Tatara and H. Fukuyama, "Resistivity Due to a Domain Wall in Ferromagnetic Metal." *Phys. Rev. Lett.* **78**, 3773 (1997).

- 32 U. Ebels, A. Radulescu, Y. Henry, L. Piraux, and K. Ounadjela, "Spin Accumulation and Domain Wall Magnetoresistance in 35 Nm Co Wires." *Phys. Rev. Lett.* **84**, 983 (2000).
- 33 R. Danneau, P. Warin, J. P. Attane, I. Petej, C. Beigne, C. Fermon, O. Klein, A. Marty, F. Ott, Y. Samson, and M. Viret, "Individual Domain Wall Resistance in Submicron Ferromagnetic Structures." *Phys. Rev. Lett.* **88**, 4 157201 (2002).
- 34 K. W. Kim, H. W. Lee, K. J. Lee, and M. D. Stiles, "Chirality from Interfacial Spin-Orbit Coupling Effects in Magnetic Bilayers." *Phys. Rev. Lett.* **111** 216601 (2013).

Figure captions

Fig. 1. (a) Schematic illustration of the film stacking. The film structure is sub.[3 W| d Ta|1 CoFeB|2 MgO|1 Ta (units in nanometer). (b) Optical micrographs of a representative wire and Hall bar with the definition of the coordinate axis. (c-f) Saturation magnetization per unit volume M_s (c), effective magnetic anisotropy energy density K_{eff} (d), anomalous Hall angle $\varphi_{\text{AHE}}^{\text{eff}}$ (e) and the spin Hall magnetoresistance (red circles) and the anisotropic magnetoresistance (blue squares) (f) plotted as a function of the Ta layer thickness d .

Fig. 2. (a) Anomalous Hall loops for two different dc currents ($I_{\text{DC}} \sim \pm 6 \text{ mA}$) for a sample with $d \sim 0.1 \text{ nm}$. The bias field along x, H_x is fixed to $\sim 1100 \text{ Oe}$. Definition of H_{eff}^z is schematically illustrated. (b) Inset: H_{eff}^z vs. I_{DC} for the same sample as in (a) with $H_x \sim \pm 1100 \text{ Oe}$. A linear function is fitted to data. The slope of the linear function divided by the current density (J_e) that flows in the HM layer is plotted against H_x in the main panel. H_{DM} is extracted from this plot as schematically drawn. ($H_{\text{DM}} \sim 200 \text{ Oe}$ here). (c) DW velocity as a function of H_x for a sample with $d \sim 0.1 \text{ nm}$. Data are fitted with a linear function and H_{DM} is estimated from the field at which the velocity is zero. (d) The DM exchange constant D plotted as a function of Ta layer thickness d . Black squares and green circles represent D obtained using the anomalous Hall loop shift measurements and the DW velocity measurements, respectively.

Fig. 3. (a) Kerr microscopy images of the magnetic states after applying an out-of-plane magnetic field H_z indicated in the left. The bright and dark regions correspond to magnetization pointing along $+z$ and $-z$, respectively (see Fig. 1(b) for the definition of the coordinate axis).

(b) Number of domain walls (black squares, left axis) and the corresponding resistance of the wire (blue circles, right axis) plotted as a function of H_z .

Fig. 4. (a) Normalized histograms of DW resistance (per one DW) ΔR . From the top, $d \sim 0.8\text{nm}$, $\sim 0.5\text{nm}$ and $\sim 0.1\text{nm}$. The number of DW resistance measurements is more than 700 for each wire. (b) Black squares show the measured DW resistance as a function of Ta layer thickness d . The error bars correspond to standard deviation of the histograms. The green circles represent calculated ΔR due to contribution from the anomalous Hall effect. The broken line shows the range of ΔR when AMR and SMR contributions are taken into account: the upper blue and lower red limit correspond to ΔR when the DW is Néel and Bloch walls, respectively.

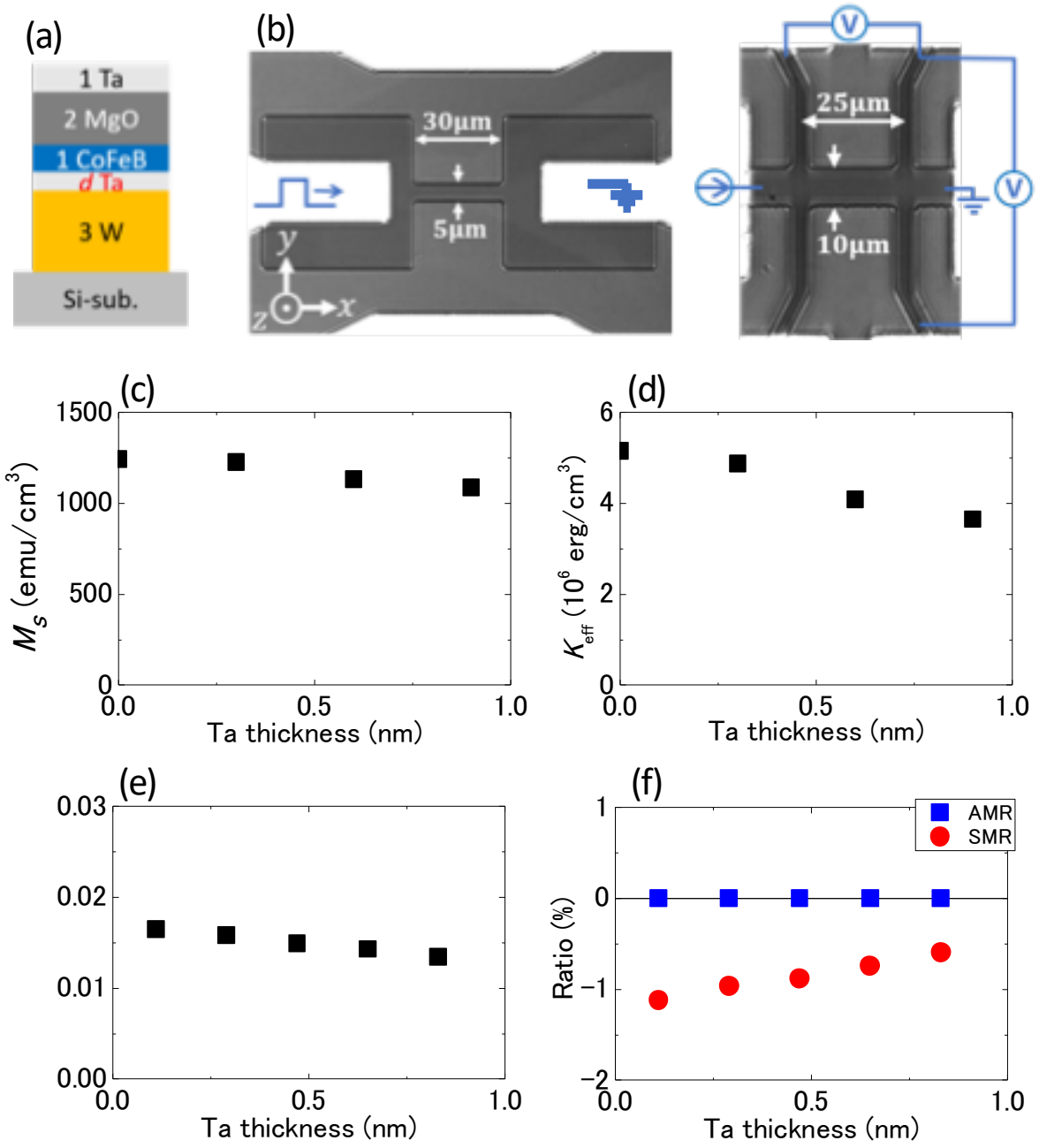


Fig. 1

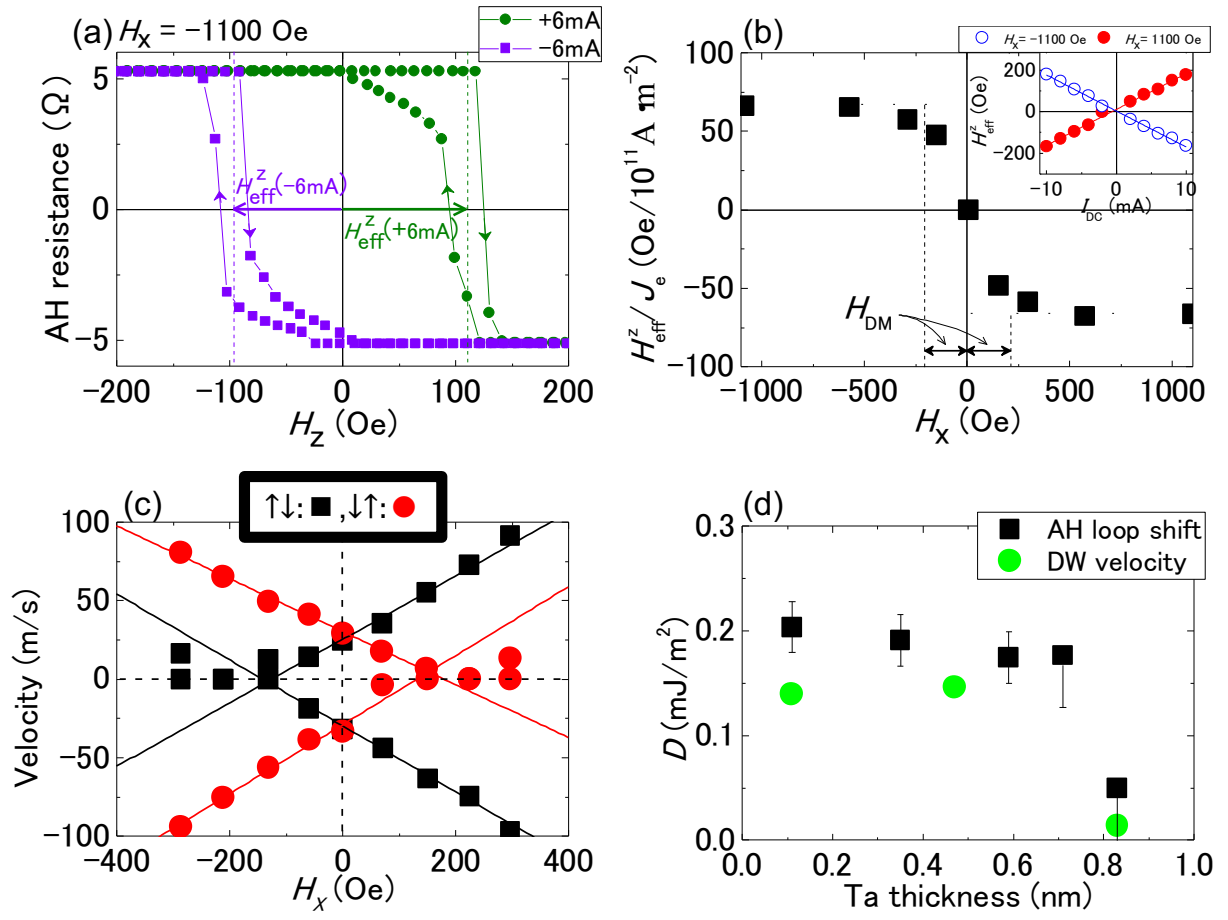


Fig. 2

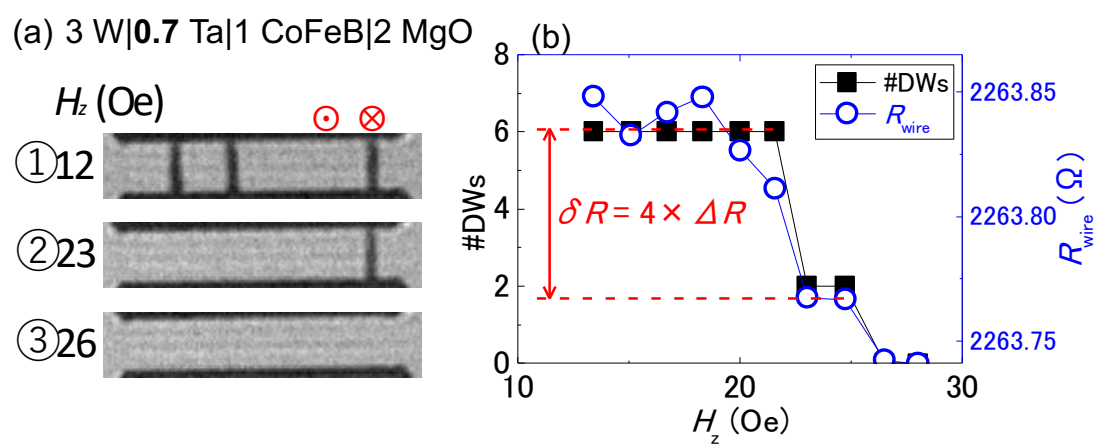


Fig. 3

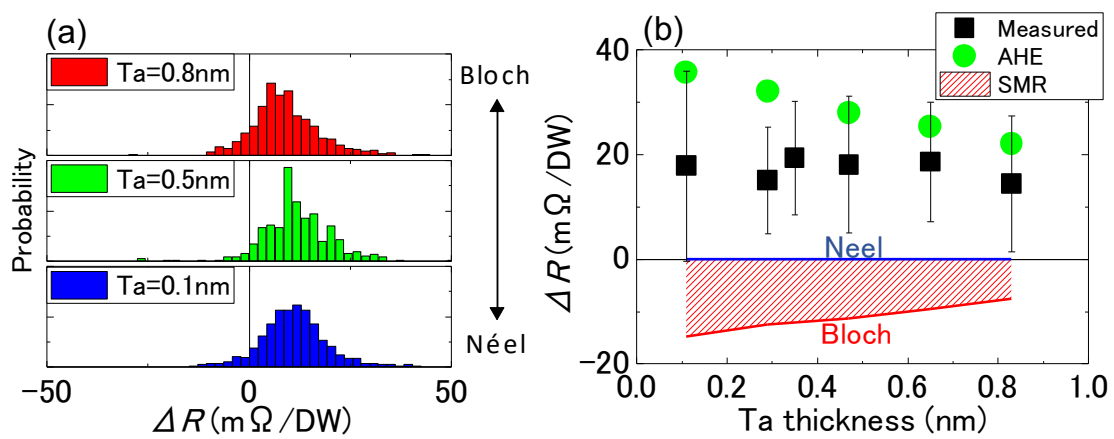


Fig. 4